Journal of Environmental Chemical Engineering 14 (2026) 122338

Contents lists available at ScienceDirect

Journal of Environmental Chemical Engineering

journal homepage: www.elsevier.com/locate/jece

Optimized continuous bioproduction of ectoine from carbon dioxide and industrial contaminants using *Guyparkeria halophila*

E. Huang-Lin [a,b], S. Cantera [a,b,*], R. Lebrero [a,b,*]

[a] Department of Chemical Engineering and Environmental Technology, University of Valladolid, Paseo Prado de la Magdalena 3-5, Valladolid 47011, Spain
[b] Institute of Sustainable Processes, University of Valladolid, Paseo Prado de la Magdalena 3-5, Valladolid 47011, Spain

ARTICLE INFO

Keywords:
C1 valorization
Extremolytes
Green pharmaceutical synthesis
Halophiles
Thiosulfate-oxidation

ABSTRACT

The production of high-value compounds such as ectoine in the pharmaceutical industry faces significant challenges, including high costs, resource intensity and reliance on refined sugars. This study presents a novel bioproduction platform converting carbon dioxide (CO_2) and the industrial contaminant thiosulfate ($S_2O_3^{2-}$) into ectoine using the halophilic strain *Guyparkeria halophila*. To overcome limitations in biomass accumulation and incomplete $S_2O_3^{2-}$ oxidation, cultivation and operational parameters, including $S_2O_3^{2-}$ loading rate, pH, and dilution rate, were systematically optimized in continuous stirred tank reactors. A $S_2O_3^{2-}$ loading rate of 5 g d^{-1} supported higher specific ectoine accumulation and promoted complete $S_2O_3^{2-}$ oxidation, while a moderate pH increase up to 7.6 further improved CO_2 assimilation. Additionally, implementing a prior semi-batch operation followed by a low dilution rate stage (0.10 d^{-1}) effectively enhanced biomass and ectoine productivity. Under these optimized conditions, biomass accumulation increased significantly to 290.0 ± 20.2 mg L^{-1}, with specific ectoine contents of 387.3 ± 23.1 mg_{Ect} $g_{biomass}^{-1}$ and productivities of 10.6 ± 0.6 g_{Ect} m^{-3} d^{-1}. This work demonstrated a scalable, efficient and sustainable platform for ectoine biosynthesis that integrates CO_2 valorization and industrial by-product utilization, highlighting the potential of halophilic microbes for greener and economically viable pharmaceutical manufacturing.

1. Introduction

In recent decades, the pharmaceutical industry has undergone remarkable expansion, emerging as one of the largest and most influential sectors in the global economy [1]. Between 2001 and 2022, global revenues surged from USD 390 billion to USD 1.48 trillion, representing nearly 280% growth [2]. However, such accelerated growth comes at the cost of significant environmental degradation. Pharmaceutical manufacturing is one of the most carbon-intensive sectors, generating significant pollutant emissions, consuming large amounts of energy and freshwater, and relying significantly on petrochemical-derived feedstocks, which bind the sector to fossil fuel dependence and aggravate climate change [3]. In fact, the global carbon footprint of the pharmaceutical sector surpasses that of several other major industries, including forestry, paper, semiconductors, and automotive, accounting for approximately 5% of worldwide greenhouse gas emissions (2.4 Gt CO_2 equivalent in 2015) [4].

In response, the European pharmaceutical strategy has emphasized green manufacturing principles, including renewable energy integration, waste minimization, and sustainable production processes [5,6]. Likewise, the growing inclination toward microbial-based manufacturing highlights microbial platforms as a promising approach for the sustainable production of high-value chemicals. Major pharmaceutical companies, including Bayer, AbbVie, Biocon, GlaxoSmithKline, Eli Lilly, Sanofi, and Merck, currently employ microbial systems for biopharmaceutical synthesis, demonstrating their industrial relevance and scalability [7]. However, a significant proportion of these bioprocesses still rely on refined sugars as carbon sources to achieve high volumetric productivities, which are costly, compete with food supply, demand large freshwater inputs, and often lead to limited economic profitability [8]. These drawbacks constrain their large-scale applicability in pharmaceutical manufacturing. In this context, microbial platforms based on C1 gases offer a potential solution by shifting from food-derived substrates to industrial waste gases such as CO_2 [9].

C1-based autotrophic platforms generally exhibit lower volumetric productivities than established heterotrophic fermentation systems and

* Corresponding authors at:Department of Chemical Engineering and Environmental Technology, University of Valladolid, Paseo Prado de la Magdalena 3-5, Valladolid 47011, Spain.
E-mail addresses: sara.cantera@uva.es (S. Cantera), raquel.lebrero@uva.es (R. Lebrero).

https://doi.org/10.1016/j.jece.2026.122338
Received 9 January 2026; Received in revised form 11 March 2026; Accepted 20 March 2026
Available online 23 March 2026

often require more complex reactor configurations to optimize gas-liquid mass transfer [10]. However, they enable the simultaneous mitigation of emissions and the biosynthesis of valuable chemicals for pharmaceutical and medical applications, such as osmolytes (ectoine, hydroxyectoine), pigments, amino acids and natural coenzymes [11]. Moreover, it enhances cost-effectiveness by reducing expensive feedstock requirements, improves resource utilization by avoiding energy-intensive pre-treatment steps and aligns with emission mitigation goals [12].

Autotrophic C1-based bioprocesses therefore involve a trade-off between potentially higher capital investment and reduced feedstock costs. Nevertheless, low-cost carbon sources such as CO_2 and industrial waste streams remain attractive for sustainable biomanufacturing. In particular, CO_2 represents a promising feedstock due to its abundance and accessibility in several industrial streams. CO_2 is inexpensive, non-toxic, and can be redirected into microbial fixation processes, providing a readily available carbon source for microbial platforms [13].

Beyond CO_2, industrial effluents may also contain other residual compounds such as carbon monoxide (CO), reduced sulfur derivatives, ammonia, and metals, which appear in either gaseous or aqueous streams and require adequate treatment before discharge [14]. Industrial effluents, including wastewater streams, often occur as complex matrices that may also contain co-contaminants such as hydrocarbons and heavy metals, which can influence contaminant migration, distribution and treatment performance in industrial sites [15]. Notably, several of these by-products can serve as direct energy sources for microbial fixation, further enhancing process sustainability and enabling the production of biomass with potential for conversion into valuable pharmaceutical ingredients. For instance, thiosulfate ($S_2O_3^{2-}$), a reduced sulfur compound frequently generated as a by-product of mining, petrochemical and wastewater treatment operations and typically present alongside other co-contaminants, where concentrations often exceed 3000 mg L^{-1}, represents a particularly abundant and relevant substrate [16]. However, if improperly managed, $S_2O_3^{2-}$ can form hazardous compounds such as hydrogen sulfide (H_2S), highlighting the urgent need for effective valorization strategies [16]. Recent studies have highlighted the rapid progression of C1-based and waste valorization microbial platforms, enabling the development of sustainable bioprocesses for the production of high-value compounds from industrial waste streams [1,12,17–19].

Within this framework, ectoine (1,4,5,6-tetrahydro−2-methyl−4-pyrimidinecarboxylic acid) stands out as a key target for sustainable bioproduction. Synthesized by halophilic and halotolerant microorganisms, this cyclic amino acid derivative functions as a compatible solute with broad protective capacities. Ectoine contributes to the stabilization of proteins, nucleic acids, and lipid membranes, and additionally acts as both a DNA protectant and cryoprotectant. Beyond its role in cellular homeostasis, ectoine has demonstrated therapeutic potential for intestinal dysfunction, pulmonary inflammation, respiratory pathologies, hypersensitivity reactions, cancer, neurodegenerative disorders, and dermatological conditions [20–22]. These multifunctional properties have consolidated ectoine as a high-value biotechnological product with applications in cosmetics (anti-aging and moisturizing formulations), pharmaceuticals (cytoprotective therapies) and agriculture (enhancement of crop stress tolerance) [23]. Its industrial importance is underscored by an estimated global demand of ~15,000 t and a market price of approximately 1000 USD kg^{-1}, with projections suggesting continued growth [24].

Recent studies have demonstrated the potential of previously unexplored halophilic and halotolerant sulfur-oxidizing bacteria as efficient ectoine producers capable of coupling CO_2 fixation with the valorization of industrial contaminants such as $S_2O_3^{2-}$. In particular, the strain *Guyparkeria halophila* has demonstrated exceptional performance, achieving ectoine accumulation of up to 47% of cellular dry weight (the highest reported among natural organisms) when grown in 15% NaCl [25]. These findings underline the potential of a novel microbial platform focused on the sustainable production of pharmaceuticals directly from CO_2 and $S_2O_3^{2-}$. Nevertheless, the process efficiency and scalability of this platform is challenged by low biomass yields and the accumulation of elemental sulfur (S^0), resulting from incomplete $S_2O_3^{2-}$ oxidation pathways [25]. Therefore, optimizing cultivation conditions to increase biomass concentration, along with developing operational strategies for continuous ectoine production in bioreactors, are crucial steps to ensure the technical and economic viability of the process.

In this context, the primary aim of this study is to explore strategies to overcome these limitations during the continuous production of ectoine from CO_2 and $S_2O_3^{2-}$ in stirred-tank bioreactors (STR) using the strain *Guyparkeria halophila*. Key operational parameters, including $S_2O_3^{2-}$ loading rates, pH, and dilution rates, were systematically evaluated to identify optimal conditions for maximizing biomass yield, CO_2 consumption, ectoine productivity and overall process performance.

2. Materials & methods

2.1. Medium and inoculum preparation

Ammonium Mineral Salt (AMS) medium supplemented with vitamins was employed as the liquid medium for both inoculum preparation and bioreactor cultivation according to Huang-Lin et al. [25]. NaCl was incorporated at concentrations of 60 or 100 g L^{-1} for inoculum activation and salinity adaptation, and 150 g L^{-1} for bioreactor operation, corresponding to the optimal salinity for ectoine production of the selected strain [21]. The medium was sterilized by autoclaving at 121 °C and 1.5 atm for 20 min. After sterilization, 100 mM $Na_2S_2O_3$ was added, and the pH was adjusted to 7.0 using a 3 M NaOH solution.

The initial bioreactor inoculum was prepared with the aerobic, halophilic thiosulfate-oxidizing strain *Guyparkeria halophila* DSM 6132, previously identified as an efficient ectoine producer [25]. The strain was acquired as an actively growing culture from DSMZ (Leibniz-Institut, Germany). For inoculum preparation, 1 mL of stock culture was inoculated, in triplicate, into 120 mL glass serum bottles containing 50 mL of AMS medium with 6% NaCl (60 g L^{-1}). Bottles were sealed with gas-tight butyl septa and aluminium caps, and the headspace was filled with 10% CO_2 and 90% air (v/v). Cultures were incubated at 37 °C under orbital shaking at 150 rpm.

Once cultures reached exponential growth, they were transferred to new glass serum bottles containing fresh AMS medium supplemented with 10% NaCl (100 g L^{-1}), and subsequently with 15% NaCl (150 g L^{-1}), following the same preparation method. This adaptation procedure was repeated three consecutive times to ensure complete acclimatization of the cultures to 15% NaCl. After reaching active growth, the *G. halophila* culture was used as inoculum for the continuous bioreactor.

2.2. Experimental set-up

Continuous process optimization was conducted in a 2.5 L STR controlled by a Sartorius Stedim Biostat®A unit (Goettingen, Germany), which enabled precise process regulation and real-time monitoring of pH and temperature (Fig. 1). The vessel was equipped with a temperature sensor and a digital pH probe. Continuous stirring at 150 rpm was provided with a six-blade Rusthon turbine and a heating blanket was used to maintain the reactor temperature at 37°C throughout the entire experiment. The pH of the culture broth was controlled through the automated addition of 2 M NaOH. The STR was initially filled with 1.7 L of sterile AMS containing 15% NaCl and 300 mL of the inoculum prepared as described in Section 2.1.

A CO_2-O_2-N_2 gas mixture (concentrations shown in Table 1) was continuously fed to the STR via a stainless-steel porous diffuser (2 µm, Supelco, USA). The empty bed residence time (EBRT) was maintained at 120 min by controlling the inlet flow rate of the gas mixture at 16 mL min^{-1}, regulated by calibrated rotameters (Aalborg, USA) before

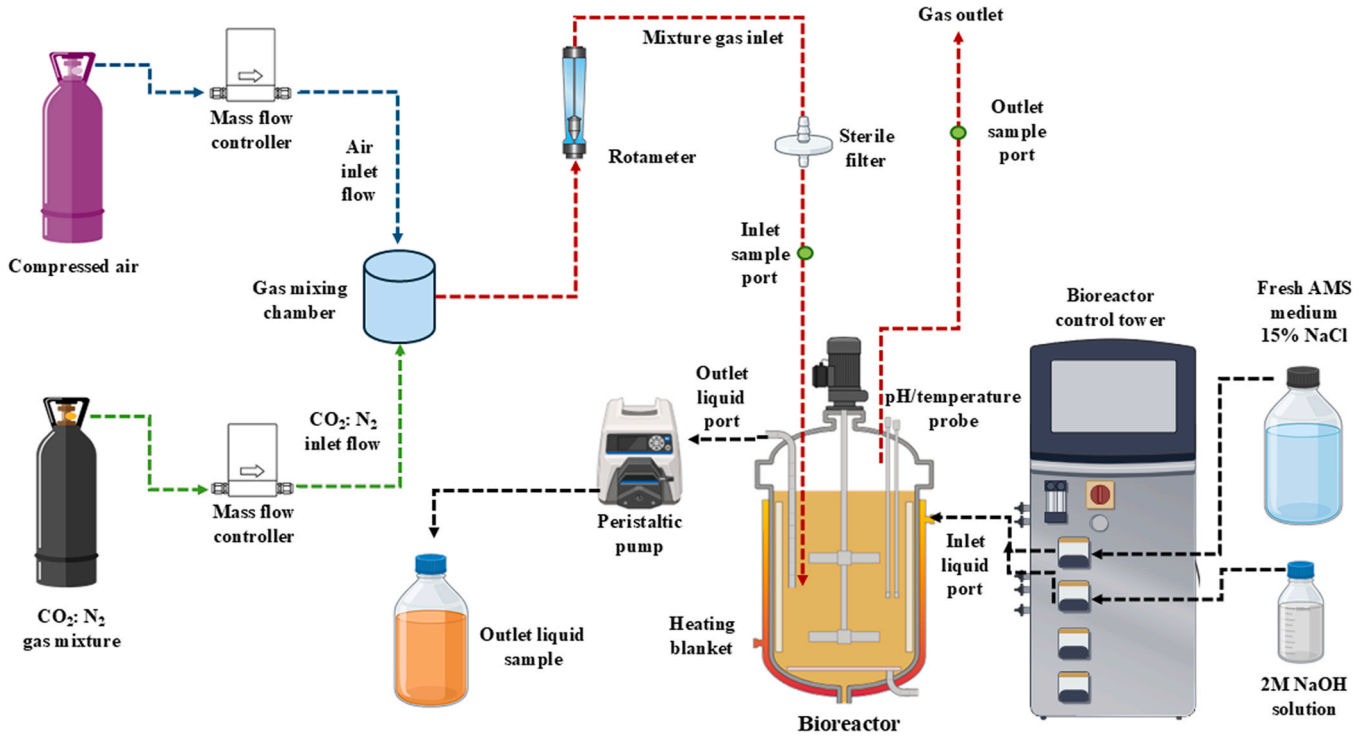

Fig. 1. Schematic diagram of the experimental set up. The diagram shows the configuration of the experimental setup used for continuous operation.

Table 1
Experimental conditions during bioreactor operation.

Operational Stage	Inlet gas flow rate (mL min^{-1})	CO_2 inlet concentration (g m^{-3})	O_2 inlet concentration (g m^{-3})	EBRT (min)	$S_2O_3^{2-}$ loading rate (g d^{-1})	Dilution rate (d^{-1})	pH	Run duration (days)
1st Biomass accumulation	15.9 ± 0.2	57.6 ± 1.3	65.8 ± 1.7	120	–	–	7.3 ± 0.1	4
I	15.8 ± 0.9	55.6 ± 4.1	64.9 ± 3.0	120	5.0	0.25	7.3 ± 0.1	7
II	15.9 ± 0.3	55.4 ± 4.5	59.6 ± 3.3	120	10.0	0.25	7.3 ± 0.2	18
III	15.8 ± 0.6	51.9 ± 3.6	55.3 ± 1.0	120	7.5	0.25	7.4 ± 0.2	16
IV	16.2 ± 0.6	59.9 ± 4.9	55.2 ± 1.9	120	7.5	0.25	7.3 ± 0.1–8.0 ± 0.2	14
2nd Biomass accumulation (semi-batch)	15.9 ± 0.1	52.5 ± 2.5	62.6 ± 0.5	120	–	1 L exchange (days 4, 8), 300 mL exchange (days 11, 13 and 15).	7.5 ± 0.1	17
V	15.9 ± 0.1	54.5 ± 1.5	65.9 ± 0.9	120	5.0	0.1	7.6 ± 0.1	23

entering the bioreactor. The gas mixture was generated by combining a 30% CO_2:70% N_2 (v/v) stream with a continuous air flow. The CO_2:N_2 stream was supplied via a mass flow controller (Aalborg, USA) and homogenized in a mixing chamber with the continuous air flow, also regulated by a mass flow controller (Aalborg, USA). To minimize the risk of contamination, 0.22 µm air filters were installed in the inlet gas stream.

CO_2 and O_2 concentrations were daily monitored to quantify consumption rates by *G. halophila*. Gas samples were collected from the inlet and outlet ports of the bioreactors using a 100 µL gas-tight syringe (Hamilton, Australia). Steady-state conditions were assumed once the oxygen elimination capacity (O_2-EC) deviated by less than 10% from the mean value for at least five consecutive days.

The liquid medium exchange was performed daily using an automated inlet pump to introduce fresh AMS medium containing 15% NaCl into the bioreactor. Simultaneously, an equivalent volume of the culture was withdrawn using a peristaltic pump (Watson Marlow, USA), maintaining a constant working volume. From the withdrawn liquid culture, 30 mL were collected daily with a 50 mL sterile syringe to assess biomass dry weight, dissolved inorganic carbon (DIC), pH, and ectoine content.

2.3. Experimental design

The experimental study was conducted in multiple operational stages to optimize biomass production, $S_2O_3^{2-}$ oxidation, CO_2 consumption and ectoine contents (Table 1). Initially, the effect of $S_2O_3^{2-}$ loading rates was evaluated during Stages I, II, and III to identify the optimal conditions for ectoine production and $S_2O_3^{2-}$ oxidation. In Stage IV, the pH was gradually increased to assess its impact on CO_2 consumption. Finally, Stage V focused on biomass accumulation, combining the optimal conditions determined in the previous stages with a reduced dilution rate to achieve overall process optimization.

Prior to the staged experiments, a 4-day biomass accumulation phase was carried out in the bioreactor. Following inoculation, the culture was allowed to fully consume the initially supplied $Na_2S_2O_3$ (100 mM), preparing the system for the subsequent staged operation.

In Stages I, II, and III, $S_2O_3^{2-}$ loading rates of 5.0, 10.0, and 7.5 g d^{-1}

were applied, respectively, while maintaining a constant dilution rate of 0.25 d^{-1}. During these stages, 500 mL of the culture medium were replaced daily with fresh 15% AMS medium containing the corresponding $Na_2S_2O_3$ concentration (40, 80, and 60 mM, respectively) which are equivalent to 1.8, 3.7 and 2.8 g L^{-1} of Na^+, respectively. Stage IV consisted of a gradual pH increase from 7.3 to 8.0, maintaining a constant dilution rate (0.25 d^{-1}) and a $S_2O_3^{2-}$ loading rate of 7.5 g d^{-1}, to evaluate its effect on CO_2 consumption.

Before initiating Stage V, biomass was allowed to accumulate under semi-batch operation to increase biomass concentration for 17 days, while the gas phase was maintained under continuous flow. Following the consumption of the initial 100 mM $Na_2S_2O_3$, 1 L of culture medium was replaced on days 4 and 8 with fresh 15% AMS supplemented with 100 mM $Na_2S_2O_3$ to ensure nutrient availability and sustain cellular activity. This approach aimed to supply fresh nutrients, remove accumulated metabolites, and reactivate cellular activity. From day 11 of Stage V, 300 mL of medium were replaced every two days to allow further biomass accumulation while minimizing dilution, thereby achieving higher biomass concentration. Stage V then focused on process optimization by controlling the pH at 7.6, reducing the dilution rate to 0.10 d^{-1} and applying a $S_2O_3^{2-}$ loading rate of 5 g d^{-1}. To this end, 200 mL of the culture medium were replaced daily with fresh 15% AMS medium containing 100 mM $Na_2S_2O_3$.

2.4. Analytical procedures

2.4.1. Ectoine determination

Intracellular ectoine was extracted from 4 mL of culture broth according to the procedure described by Cantera et al. [26]. Ectoine analysis was performed by HPLC-UV using a Waters Alliance e2695 system equipped with a 717 Plus autosampler (Waters, USA) and a Dual λ Absorbance detector (Waters, USA) set at 220 nm and 40 °C. Separation was achieved on a Spherisorb Amino (NH_2) Column, 80 Å, 3 μm, 4.6 mm × 150 mm (Waters, USA). Acetonitrile:Water 75%:25% (v/v) was used as the mobile phase at a flow rate of 0.6 mL min^{-1}. Quantification was carried out using external calibration curves prepared with commercial ectoine [(S)-β−2-methyl−1,4,5,6-tetrahydropyrimidine−4-carboxylic acid, 95% purity] (Sigma-Aldrich, Spain). The specific intracellular ectoine content was then calculated as described in Eq. 1.

$$[Ect\ SP]\left(\frac{mg\ ect}{g\ biomass}\right) = \frac{\text{mg intra} - \text{cellular ectoine}}{\text{dry weight biomass}} \quad (1)$$

2.4.2. Thiosulfate and sulfate quantification

$S_2O_3^{2-}$ and sulfate (SO_4^{2-}) concentrations were determined by HPLC-IC (Waters, Bellefonte, USA) equipped with a Waters 432 ionic conductivity detector and an IC-Pak Anion HC column (150 mm × 4.6 mm; Waters, Bellefonte, USA). Daily, 1 mL samples from the bioreactor culture were collected, filtered through 0.22 μm membranes, transferred into HPLC vials, and stored at −20 °C until analysis. Quantification of $S_2O_3^{2-}$ and SO_4^{2-} was carried out using calibration curves prepared with standard solutions ranging from 1.0 to 30.0 g L^{-1}. The sulfur mass balance was subsequently calculated according to Eq. (2), as described by Houghton et al. [27].

$$S_2O_3^{2-} + 2\ O_2\ (aq) + H_2O \rightarrow 2\ SO_4^{2-} + 2\ H^+ \quad (2)$$

2.4.3. Carbon dioxide and oxygen monitoring

CO_2 and O_2 concentrations were analyzed using an Agilent 7890 A GC-TCD system (Agilent Technologies, USA) equipped with a CP Poraplot Q column (CP7554, 25 m × 0.53 μm × 20 μm). The oven, injector, and detector temperatures were maintained at 45 °C, 150 °C, and 200 °C, respectively. Helium was employed as the carrier gas at a flow rate of 13.7 mL min^{-1}. DIC in the aqueous phase was quantified using a TOC-VCSH total organic carbon analyzer (Shimadzu, Japan). Prior to analysis, samples were filtered through 0.22 μm filters and adjusted to pH 9 with 0.5 M NaOH. The total CO_2 content was calculated as the sum of CO_2 concentrations in both the gas and aqueous phases.

2.4.4. Biomass determination

Biomass growth was monitored by measuring the optical density at 600 nm (OD_{600}) using a SPECTROstar Nano spectrophotometer (BMG LABTECH, Germany). Dry biomass concentration was determined as total suspended solids (TSS) following Standard Methods [28]. Medium pH was measured with a SensION™ + PH3 pH meter (HACH, Spain).

2.4.5. Microbial broth purity assessment

Purity check amplicon metagenomic analyses were performed to assess potential microbial contamination. At the end of operational Stages IV and V, 10 mL of bioreactor culture were collected in triplicate. DNA was extracted from each biological replicate using the FastDNA™ SPIN Kit for Soil (MP Biomedicals, USA). The 16S rRNA gene (V4-V5 regions) was PCR-amplified with universal primers containing specific barcodes. Sequencing libraries were prepared with the TruSeq® DNA PCR-Free Sample Preparation Kit, and their quality was assessed using a Qubit® 2.0 Fluorometer and an Agilent Bioanalyzer 2100 system. Libraries were then pooled, quantified, and sequenced on an Illumina paired-end platform, producing 250 bp raw paired-end reads at Novogene UK (Cambridge, UK).

Raw reads were merged using FLASH (v1.2.11) [29]. Data filtering and chimera removal were performed with Fastp (v0.23.1) [30] and the VSEARCH package (v2.16.0) [31]. Taxonomic annotation was carried out with QIIME2 against the SILVA database (v138.1). Finally, bar plots were generated in R using the ggplot2 package [32] and 16S rRNA sequencing data were deposited in NCBI under BioProject accession PRJNA1353889 and BioSample accessions SAMN52937313, SAMN52937314, SAMN52937315, SAMN52937316, SAMN52937317, SAMN52937318 (Stage IV_1–IV_3 and Stage V_1–V_3).

2.4.6. Statistical Analysis

Statistical analyses were performed using SPSS 26.0 (IBM, USA). ANOVA followed by post-hoc tests was used for multiple group comparisons, considering homoscedasticity or heteroscedasticity based on Levene's test. Differences were considered significant at $p < 0.05$. Bioreactor experiments were conducted as single continuous runs for each operational stage. Daily measurements were treated as independent observations for statistical evaluation. Analytical determinations (ectoine, thiosulfate, sulfate, gas composition and biomass concentration) were performed at least in duplicate. Results are expressed as mean ± standard deviation (SD).

3. Results and discussion

3.1. Influence of thiosulfate loading rates on bioreactor performance (Stage I-III)

The results obtained during operational Stages I–III of the bioreactor are summarized in Fig. 2. Prior to continuous operation, a biomass accumulation phase was conducted by inoculating the reactor with an actively growing culture of *G. halophila* at an initial concentration of 36.0 ± 1.3 mg L^{-1}, under pH conditions of 7.0 ± 0.1, and 15% AMS (Fig. 2b). During this phase, a lag period of three days was observed. Biomass increased steadily until the 100 mM of $Na_2S_2O_3$ supplied were completely consumed. By day 4, biomass reached a concentration of 86.0 ± 10.2 mg L^{-1}.

Stage I initiated with continuous operation at a dilution rate of 0.25 d^{-1} and a $Na_2S_2O_3$ loading rate of 5 g d^{-1}. Under these conditions, biomass exhibited a significant increase, reaching a maximum concentration of 210.0 ± 19.5 mg L^{-1} on day 5, along with specific ectoine contents of 150.1 ± 7.3 $mg_{Ect}\ g_{biomass}^{-1}$. In parallel, CO_2 removal efficiency

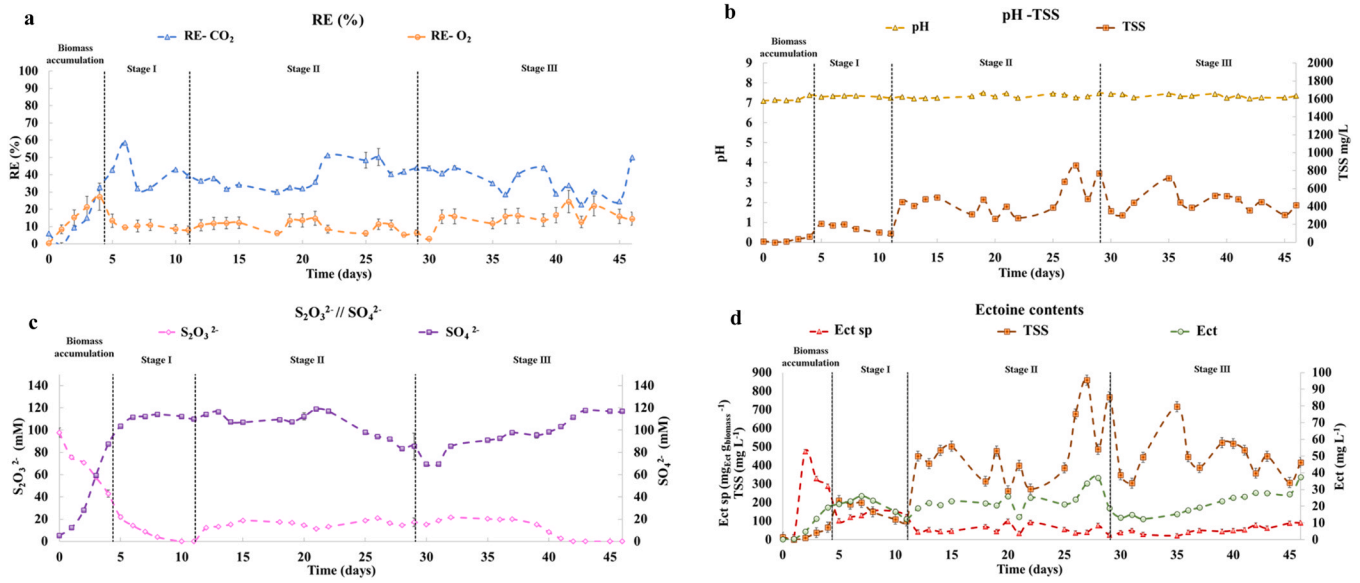

Fig. 2. Effect of thiosulfate loading rate on reactor performance during operational Stages I-III. (a) Removal efficiencies (RE, %) obtained during Stages I-III: RE-CO_2 (blue dashed line) and RE-O_2 (orange dashed line); (b) pH values (yellow dashed line) and biomass concentrations (orange dashed line); (c) Thiosulfate and sulfate outlet concentrations: $S_2O_3^{2-}$ concentration (purple dashed line); SO_4^{2-} concentration (pink dashed line); (d) Specific ectoine content (red dashed line); ectoine concentration (green dashed line) and biomass concentration (orange dashed line). Vertical black dashed lines indicate initiation of each operational stage. Data are presented as mean values (n = 3). Error bars represent standard deviation (SD).

peaked on day 6 at 55.3 ± 4.1% and subsequently stabilized at an average value of 36.8 ± 5.4%. However, from day 6 onwards, biomass concentrations declined significantly, dropping to 100.5 ± 3.9 mg L^{-1} by day 10, concurrent with the complete depletion of $S_2O_3^{2-}$ in the culture broth and resulting in an average SO_4^{2-} concentration of 114.1 ± 1.3 mM. Notably, despite the reduction in biomass, ectoine levels remained stable, with mean values of 153.3 ± 62.0 mg_{Ect} $g_{biomass}^{-1}$ This behaviour likely reflected a stress-induced metabolic adaptation, in which, during limited $S_2O_3^{2-}$ availability, cellular resources including metabolic precursors and energy, may be preferentially allocated to ectoine biosynthesis at the expense of biomass production [33].

To overcome the $S_2O_3^{2-}$ limitation that likely constrained biomass growth during Stage I, the $S_2O_3^{2-}$ loading rate was doubled to 10 g d^{-1} in Stage II (day 11). This adjustment promoted biomass accumulation, resulting in an approximately threefold rise (450.1 ± 10.1 mg L^{-1}). Despite this enhanced growth, CO_2 removal remained relatively stable (39.1 ± 7.1%) while specific ectoine yield decreased to 41.9 ± 5.4 mg_{Ect} $g_{biomass}^{-1}$ under these conditions. Such decline suggests that most of the assimilated carbon is preferentially allocated to biomass formation rather than diverted toward secondary metabolite pathways, thereby diminishing the carbon flux available for ectoine biosynthesis. Furthermore, the elevated $S_2O_3^{2-}$ loading rate unexpectedly induced an incomplete oxidation pathway, as evidenced by the accumulation of S^0 observed in the bioreactor and residual $S_2O_3^{2-}$ in the effluent (average concentrations of 15.8 ± 2.8 mM). Previous pangenomic analysis revealed that *G. halophila* possesses the complete Sox pathway for $S_2O_3^{2-}$ oxidation to SO_4^{2-} as final product [34]. Nonetheless, as reported for other sulfur-oxidizing bacteria such as *Thiomicrospira thermophila*, sub-optimal conditions (limited O_2 concentrations or acidic pH) can shift metabolism toward incomplete oxidation, leading to partially oxidized sulfur species or intracellular S^0 accumulation [27]. A theoretical oxygen transfer analysis (Supplementary Materials 1) demonstrated that, under the applied $S_2O_3^{2-}$ loading rate (10 g d^{-1}), the stoichiometric oxygen demand (OUR) exceeded the estimated oxygen transfer capacity (OTR) of the reactor (OTR/OUR < 1). Under these conditions, oxygen transfer likely acted as a physical constraint, limiting complete oxidation and promoting the formation of partially oxidized sulfur species.

To optimize performance based on previous stages, $S_2O_3^{2-}$ loading rate was adjusted to 7.5 g d^{-1} in Stage III (day 29). During this stage, biomass concentrations remained comparable to those recorded in Stage II (460.9 ± 69.3 mg L^{-1}), while specific ectoine contents showed no significant increase, remaining at average values of 50.0 ± 19.1 mg_{Ect} $g_{biomass}^{-1}$. This trend aligns with the metabolic limitation previously discussed, in which most of the fixed carbon could be directed toward biomass formation rather than ectoine biosynthesis. The accumulation of S^0 gradually decreased throughout the stage, as indicated by the absence of visible sulfur precipitation, and by its end, the supplied $S_2O_3^{2-}$ was completely consumed. However, the persistence of an incomplete oxidation pathway was evidenced by a significant deviation from the stoichiometrically predicted sulfur mass balance, with lower-than-expected SO_4^{2-} yields (as predicted by Eq.2), suggesting that a fraction of $S_2O_3^{2-}$ was still diverted into intermediate or partially oxidized sulfur species. Although the $S_2O_3^{2-}$ loading rate was reduced compared to Stage II, the calculated OTR/OUR ratio remained below unity (Supplementary Materials 1), suggesting that oxygen transfer constraints likely continued to limit sulfur oxidation efficiency. Consequently, complete oxidation was not fully restored under these operational conditions.

Based on the results observed in Stages I to III, limited $S_2O_3^{2-}$ availability in Stage I promoted complete oxidation to SO_4^{2-} and maximized specific ectoine accumulation, although overall productivity remained limited due to low biomass concentrations (5.1 ± 1.2 g_{Ect} m^{-3} d^{-1}). In contrast, higher $S_2O_3^{2-}$ loading rates in Stage II enhanced biomass growth but induced incomplete thiosulfate oxidation, resulting in S^0 formation, residual $S_2O_3^{2-}$, and decreased specific ectoine content. Adjusting the $S_2O_3^{2-}$ loading rate to 7.5 g L^{-1} in Stage III improved $S_2O_3^{2-}$ utilization and partially restored the complete oxidation pathway, although ectoine levels remained similar to those of Stage II. Overall, these findings indicate that the $S_2O_3^{2-}$ loading rate applied in Stage I represents the most

favourable conditions for balancing $S_2O_3^{2-}$ oxidation and ectoine biosynthesis.

3.2. Impact of pH on CO_2 consumption and process stability (Stage IV)

Enhancing inorganic carbon availability represents a critical factor for optimizing autotrophic growth [35]. Since the solubility of CO_2 in aqueous systems is strongly influenced by pH, a controlled increase in pH can shift the carbonate equilibrium [35,36], thereby increasing the concentration of DIC available for fixation via the Calvin-Benson cycle in *G. halophila* [34].

To further enhance CO_2 bioavailability, Stage IV evaluated the effect of gradually increasing the pH from 7.3 to 8.0, approaching the upper growth tolerance value of *G. halophila* [37]. The same dilution rate (0.25 d^{-1}) and $S_2O_3^{2-}$ loading rate (7.5 g d^{-1}) as in Stage III were maintained, starting from a relatively high biomass concentration (265.0 ± 13.2 mg L^{-1}). The results of Stage IV are summarized in Fig. 3. During this stage, total CO_2 removal, accounting for both gaseous and carbonate fractions, increased significantly, with average removals of 51.6 ± 3.1%, nearly 10% higher than in previous stages (Fig. 3a). Concomitantly, specific ectoine contents increased significantly compared to previous stages, achieving maximum values of 190.7 ± 33.7 mg_{Ect} $g_{biomass}^{-1}$ by day 55 when operating at a pH of 7.6 (Fig. 3d). This enhancement was attributed to increased CO_2 assimilation, which alleviated the previous constraint on carbon allocation toward secondary metabolite synthesis.

Under these conditions, the combination of abundant reducing power and ATP derived from $S_2O_3^{2-}$ oxidation and higher carbon availability allowed the metabolic flux to be

effectively redirected toward ectoine biosynthesis. However, at pH values higher than 7.6, biomass concentration began to decline significantly (Fig. 3b), decreasing from 350.0 ± 16.1 mg L^{-1} on day 49–195.1 ± 3.3 mg L^{-1} on day 59. Specific ectoine levels followed a similar trend, dropping by day 55 and reaching 148.5 ± 5.1 mg_{Ect} $g_{biomass}^{-1}$ at pH 8.0 (day 59).

Consequently, the average ectoine productivity during this stage was 5.2 ± 1.5 g_{Ect} m^{-3} d^{-1}. This decline may be attributed to the non-alkalophilic nature of *G. halophila*: although it can tolerate growth at pH values up to 8.0, its optimal growth occurs at pH 7.0, with metabolic activity progressively constrained at higher pH. These results align with findings for the non-alkalophilic *Piscibacillus halophilus*, where ectoine accumulation peaked at pH 7.5 and decreased at higher pH values [38]. Such findings underscore the critical influence of pH on ectoine biosynthesis, as deviations from the optimal range can significantly reduce microbial growth and metabolic activity by up to 50% [39]. Concomitant with the decline in biomass and ectoine contents, $S_2O_3^{2-}$ consumption decreased, as evidenced by residual $S_2O_3^{2-}$ in the bioreactor effluent (5.2 ± 0.2 mM), while SO_4^{2-} production remained stable compared to Stage III (116.0 ± 3.7 mM) (Fig. 3c). This observation is consistent with previous reports on *Thiobacillus thiooxidans*, showing that deviations above the optimal pH significantly reduced thiosalt oxidation rates [40].

Stage IV results indicate that while a moderate increase in pH enhanced CO_2 fixation and stimulated ectoine accumulation in *G. halophila*, values above the optimal range (> 7.6) significantly limited growth and metabolic efficiency, ultimately reducing overall process performance.

3.3. Integrated optimization for biomass accumulation and ectoine production (Stage V)

In the previous operational stages, a low $S_2O_3^{2-}$ loading rate (5 g d^{-1}) was found to enhance specific ectoine accumulation and promote complete $S_2O_3^{2-}$ oxidation by *G. halophila*, while a moderate pH increase (up to 7.6) further improved CO_2 assimilation. However, biomass concentrations remained low under these conditions, thereby limiting ectoine productivities.

Therefore, the subsequent Stage V was designed to address this

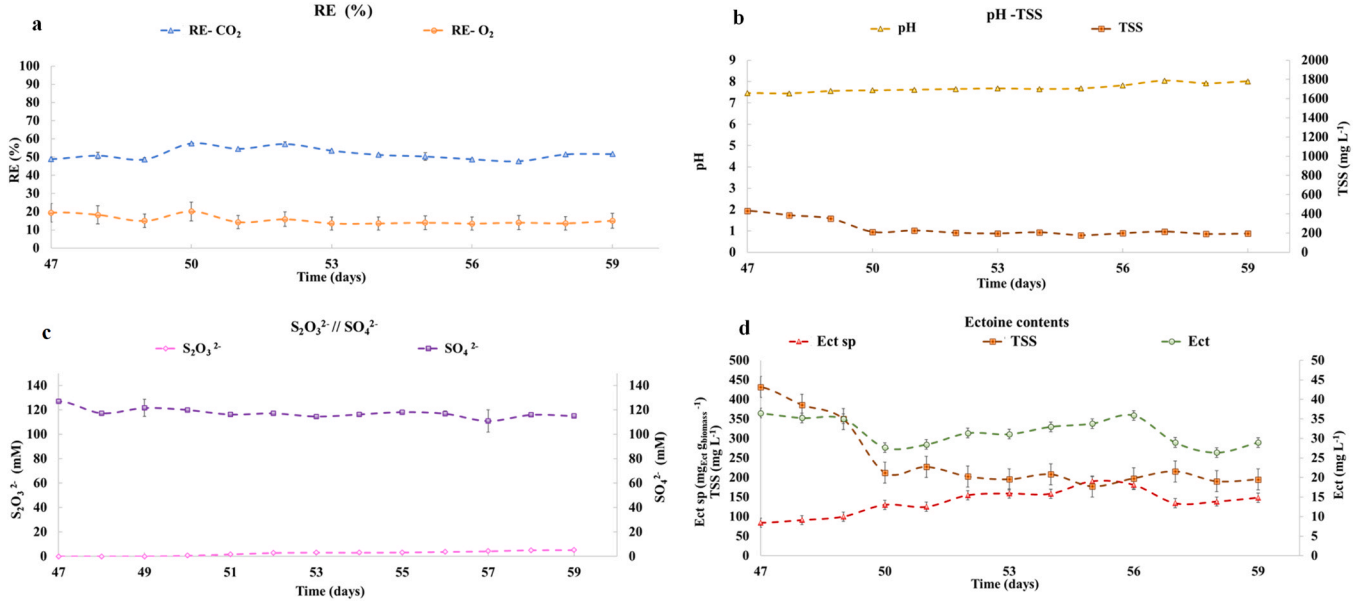

Fig. 3. Influence of pH on CO_2 consumption, biomass concentration and ectoine production during Stage IV. (a) Removal efficiencies (%) obtained during Stage IV: RE-CO_2 (blue dashed line) and RE-O_2 (orange dashed line); (b) pH values (yellow dashed line) and biomass concentrations (orange dashed line); (c) Thiosulfate and sulfate outlet concentrations: $S_2O_3^{2-}$ concentrations (purple dashed line); SO_4^{2-} (pink dashed line); (d) Specific ectoine content (red dashed line); ectoine concentration (green dashed line) and biomass concentration (orange dashed line). Vertical black dashed lines indicate initiation of each operational stage. Data are presented as mean values (n = 3). Error bars represent standard deviation (SD).

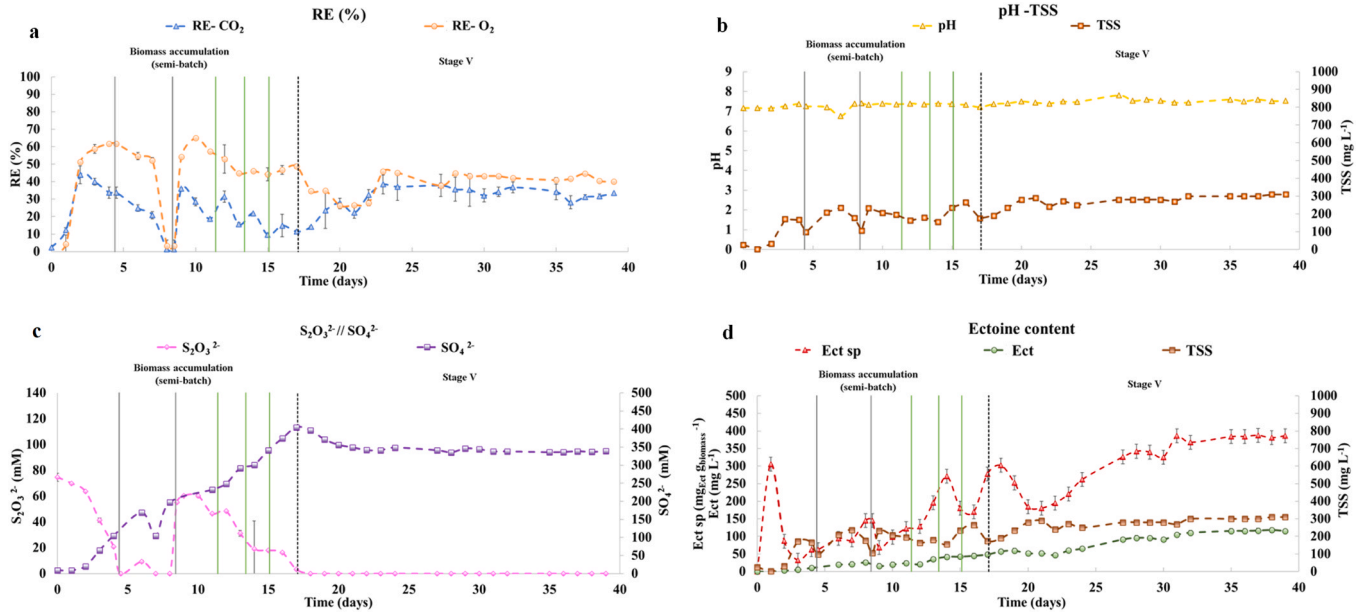

Fig. 4. Reactor performance during biomass accumulation and optimized continuous operation (Stage V). (a) Removal efficiencies (%) obtained during Stage V: RE-CO_2 (blue dashed line) and RE-O_2 (orange dashed line); (b) pH values (yellow dashed line) and biomass concentrations (orange dashed line); (c) Thiosulfate and sulfate outlet concentrations: $S_2O_3^{2-}$ concentrations (purple dashed line); SO_4^{2-} (pink dashed line). (d) Specific ectoine content (red dashed line); ectoine concentration (green dashed line) and biomass concentration (orange dashed line). Vertical grey line indicates the replacement of 1 L of fresh AMS 15%, and vertical green line the replacement of 300 mL of fresh AMS 15%. Vertical black dashed lines indicate initiation of each operational stage. Data are presented as mean values (n = 3). Error bars represent standard deviation (SD).

limitation by focusing on strategies to sustain higher biomass concentrations while applying the previously identified optimal operational parameters.

To this end, a second biomass accumulation phase was carried out prior to Stage V. This involved an initial semi-batch period aimed at promoting biomass accumulation in the reactor by maintaining a continuous gas supply while periodically replenishing the medium with $S_2O_3^{2-}$. This strategy ensured sustained nutrient and electron donor availability while keeping the culture in exponential growth [41]. As in the first accumulation phase, the culture was inoculated with an actively growing culture of *G. halophila* at 26.0 ± 2.0 mg L^{-1} under pH 7.2 ± 0.1 and 15% AMS. Here, the lag phase was reduced to 2 days. Biomass was then sustained through two initial 1 L replacements of AMS 15% supplemented with 100 mM of $Na_2S_2O_3$ on days 4 and 8, which effectively promoted growth, reaching a TSS concentration of 232.0 ± 5.1 mg L^{-1} on day 6, and an average specific ectoine content of 95.8 ± 33.4 mg_{Ect} $g_{biomass}^{-1}$. Subsequent 300 mL replacements on days 11, 13 and 15, successfully prevented washout and further enhanced biomass accumulation, achieving concentrations of 267.3 ± 2.5 mg L^{-1} by day 16, over threefold higher than the initial value obtained in Stage I (86.0 ± 2.2 mg L^{-1}). Additionally, the specific ectoine concentration increased to an average of 177.9 ± 54.4 mg_{Ect} $g_{biomass}^{-1}$, likely because the smaller replacement volume allowed the accumulated biomass to remain metabolically active without excessive dilution, balancing growth and metabolite production. These results confirmed the effectiveness of the semi-batch operation in increasing biomass concentration while enhancing ectoine contents prior to Stage V.

Stage V initiated on day 17 with the optimal operational conditions identified in previous stages: $S_2O_3^{2-}$ loading rate of 5 g d^{-1} and stable pH at 7.6 (Fig. 4).

A reduced dilution rate of 0.10 d^{-1} was applied to minimize the risk of biomass washout and sustain its retention in the bioreactor. During this stage, biomass stabilized at average concentrations of 290.0 ± 20.2 mg L^{-1}. On day 18, a significant decline in specific ectoine content was observed, decreasing from 302.0 ± 27.3–184.3 ± 21.1 mg_{Ect} $g_{biomass}^{-1}$. This reduction likely reflected a cellular adaptation response to the renewed operational conditions, which was consistent with the concurrent decrease in CO_2 assimilation (from 48.8 ± 5.2% to 34.7 ± 3.1%).

From day 21 onward, specific ectoine concentrations recovered progressively, reaching average contents of 387.3 ± 23.1 mg_{Ect} $g_{biomass}^{-1}$ by the end of the stage, coupled with CO_2 removal stabilizing at 44.8 ± 5.0%. This pronounced increase can be attributed to the combined effects of several factors. The reduced dilution rate (0.10 d^{-1}) minimized biomass washout and limited excessive growth, allowing cells to allocate more resources to ectoine biosynthesis. At the same time, abundant reducing power and ATP derived from complete $S_2O_3^{2-}$ oxidation provided a continuous supply of electrons and energy, while sustained CO_2 availability ensured sufficient carbon for both biomass production and metabolite synthesis. Because ectoine is synthesized from fixed carbon intermediates, its energetic cost is inherently included within the overall CO_2 fixation demand. Considering the Stage V $S_2O_3^{2-}$ loading (5 g d^{-1}) and the electron derived from a complete oxidation to SO_4^{2-}, the potential generation of reducing power and ATP would be expected to exceed the estimated energetic demand for CO_2 fixation and ectoine biosynthesis. Based on the electron yield from $S_2O_3^{2-}$ oxidation and the typical energetic requirements of the CBB cycle (2 NADH and 3 ATP per mol of CO_2) [42], the theoretical supply of reducing power and ATP is several-fold higher than the biosynthetic demand. This supports operation under non-energy-limited conditions and suggests that increased ectoine accumulation in Stage V was more likely linked to carbon flux redistribution rather than to energy availability. Detailed calculations are provided in Supplementary materials 2. In addition, to further validate the reliability of the steady-state data obtained in Stage V, both a Carbon Mass Balance

(CMB) and a Degree of Reduction (DoR) balance were performed (Supplementary Material 2). The CMB showed a closure of approximately 101%, confirming consistency between CO_2 consumption and carbon recovery as biomass (including intracellular ectoine) and residual DIC in the effluent. In parallel, the DoR analysis indicated that only ~3.3% of the electron equivalents derived from $S_2O_3^{2-}$ oxidation were incorporated into biomass carbon, while the remaining fraction was likely dissipated through respiratory processes to sustain ATP generation. Together, these balances indicated the absence of significant unaccounted carbon or electron sinks during Stage V operation."

Furthermore, following adaptation to the reduced dilution rate, the biomass re-established metabolic homeostasis and up-regulated biosynthetic pathways for ectoine production, enabling highly efficient intracellular accumulation. During this stage, specific ectoine contents were nearly two-folds the values obtained in previous stages and comparable to those reported by Huang-Lin et al. [19] (476.9 ± 37.1 $mg_{Ect}\ g_{biomass}^{-1}$), while the average biomass achieved in the present study (290.0 ± 20.2 mg L^{-1}) was approximately 28-fold higher than that reported in their semi-continuous system (10.3 ± 3.1 mg L^{-1}). Meanwhile, $S_2O_3^{2-}$ oxidation remained stable throughout Stage V with complete substrate consumption and no evidence of incomplete oxidation. This resulted in a stoichiometrically balanced sulfur mass profile, in which the total sulfur input as $S_2O_3^{2-}$ was quantitatively converted to SO_4^{2-}, consistent with the stoichiometry defined in Eq. 2, and an average SO_4^{2-} production of 337.7 ± 10.6 mM, nearly two-fold higher than in prior stages. Notably, the OTR/OUR ratio calculated for Stage V indicated an operation within a non-transfer-limited regime (Supplementary Materials 1). This shift in oxygen balance, together with the reduced dilution rate and optimized pH, explained the restoration of complete $S_2O_3^{2-}$ oxidation and stable reactor performance.

During this stage, the average ectoine productivity reached 10.6 ± 0.6 $g_{Ect}\ m^{-3}\ d^{-1}$, significantly exceeding the values recorded in earlier stages (Fig. 5), demonstrating the potential of lowering the dilution rate as an effective strategy. Although the daily withdrawn volume decreased, the combination of a high steady-state biomass concentration and significantly higher specific ectoine content achieved during this stage resulted in an overall increase in final ectoine productivity. Previous semi-continuous studies showed that a dilution rate of 0.08 d^{-1} maintained biomass in exponential growth, enhancing specific ectoine production but resulting in low biomass yields. Further lowering the dilution rate slightly increased biomass, while overall performance declined due to pH drop and oxygen limitation [19].

Notably, the specific intracellular ectoine concentrations achieved in this stage exceeded those reported for natural autotrophic microorganisms such as *Hydrogenovibrio marinus* DSM 11271 (134 $mg_{Ect}\ g_{biomass}^{-1}$ with CO_2 and H_2) [26] and *Methylotuvimicrobium alcaliphilum* 20Z/DSM19304 (109 $mg_{Ect}\ g_{biomass}^{-1}$ with CH_4) [43], as well as genetically engineered strains such as *Methylomicrobium alcaliphilum* 20Z (111 $mg_{Ect}\ g_{biomass}^{-1}$ with CH_4) [23] and *Halomonas hydrothermalis* Y2 (223 $mg_{Ect}\ g_{biomass}^{-1}$ with monosodium glutamate) [44]. These values also exceeded those of heterotrophic microorganisms, including *Brevibacterium epidermis* DSM 20659 (160 $mg_{Ect}\ g_{biomass}^{-1}$ with sodium glutamate and yeast extract) [45] and the industrial ectoine producer *Halomonas elongata* (100–180 $mg_{Ect}\ g_{biomass}^{-1}$ with high quality sugars) [46].

Although a significant increase in biomass concentration was achieved in the present study compared to previous works [19], the overall biomass level obtained remains insufficient to support ectoine volumetric productivities comparable to those reported for heterotrophic *Halomonas* strains. This contrast is particularly evident for engineered platforms, which reached ectoine concentrations of up to 85 g L^{-1} [47], whereas other optimized heterotrophic processes with *Halomonas* strains typically achieved 10–15 g L^{-1} under fed-batch conditions [48–50]. For instance, improving bioreactor design could contribute to enhancing ectoine productivity by supporting higher biomass accumulation. In particular, increasing gas-liquid mass transfer and implementing biomass retention strategies may overcome current limitations. The use of high mass-transfer reactors, such as pressurized stirred-tank reactors [51] or microbubble driven airlift systems [52], may facilitate improved O_2 and CO_2 transfer and thereby promote greater biomass accumulation.

Beyond reactor engineering, further optimization under complex multi-factor operational conditions may benefit from data-driven approaches. In this context, machine learning tools could facilitate the identification and prediction of nonlinear interactions among key operational parameters, enabling more robust and efficient process control [53].

3.4. Contamination control during bioreactor operation

Maintaining strain purity is critical in pharmaceutical manufacturing, as contamination can compromise product yield, process efficiency, and the reliability of results [54,55]. In this study, purity checks at the end of Stages IV and V (Supplementary Materials 3) revealed that members of the genus *Guyparkeria* accounted for approximately 99.7% of the community (Stage IV), with the remaining taxa representing less than 0.3%, a negligible level of contamination. By Stage V, the genus *Guyparkeria* constituted 100% of the community, indicating a virtually pure culture. Achieving such purity in continuous manufacturing is typically challenging due to the constant risk of contamination [56]. However, the salinity (15% NaCl) and the chemolithotrophic conditions employed in this system provides a natural selective barrier against most unwanted microorganisms. These conditions

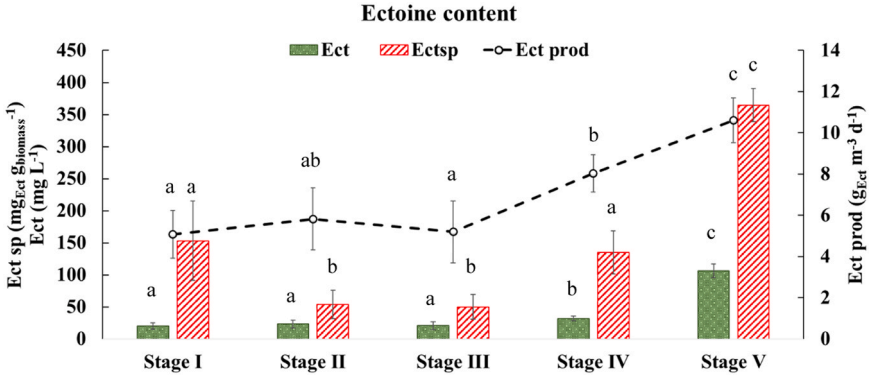

Fig. 5. Comparison of mean ectoine concentrations, ectoine productivity and specific ectoine contents across operational stages. Mean ectoine concentrations (green dotted bars), specific ectoine contents (red-hatched bars) and ectoine productivity (black dashed line) obtained during each operational stage. Data are presented as mean values (n = 3). Error bars represent standard deviation (SD). Values with different superscript letters are significantly different between each stage (ANOVA, $p < 0.05$).

may also contribute to maintaining genetic stability during continuous cultivation, as halophilic microorganisms have been reported to display high genomic stability under hypersaline conditions [57]. This feature underscores a significant advantage of halophilic platforms like *G. halophila* for industrial pharmaceutical production. The inherent resistance to contamination not only ensures process stability and reproducibility but also reduces the need for stringent sterile handling and costly decontamination procedures.

While this study focuses on upstream optimization of continuous ectoine production using *G. halophila*, industrial scale implementation of this platform will require consideration of downstream recovery of intracellular ectoine from high-salinity matrices, which remains energy-intensive. In this context, alternative recovery strategies such as bacterial milking (hypoosmotic shock) or controlled cell disruption should be considered when evaluating overall process feasibility [58,59]. Additionally, future developments may explore the use of strains with enhanced ectoine excretion capacity, including naturally "leaky" variants or engineered strains designed to facilitate extracellular release, which could significantly reduce downstream processing costs.

4. Conclusion

In this context, this study represents the first proof of concept for coupling ectoine production with the continuous abatement of CO_2 and $S_2O_3^{2-}$ using *Guyparkeria halophila* as a biocatalyst. Importantly, the results of this study provided new insights into the optimal operating conditions to promote ectoine accumulation, complete $S_2O_3^{2-}$ oxidation and improved CO_2 assimilation. In particular, the combined control of $S_2O_3^{2-}$ loading rate, pH and dilution rate enabled stable biomass accumulation and continuous ectoine production under autotrophic conditions. The specific ectoine contents achieved in this study surpass most values reported for natural production platforms. However, volumetric productivities remain lower than those typically observed in heterotrophic fermentation processes, which is consistent with the intrinsic constraints of autotrophic metabolism and gas-liquid mass transfer. Future studies focused on a detailed techno-economic evaluation will be required to determine the overall competitiveness of this process. Overall, these results demonstrate the feasibility of a continuous, sustainable bioprocess for converting CO_2 and $S_2O_3^{2-}$ into pharmaceuticals, highlighting the potential of *G. halophila* as an efficient biological platform for industrial ectoine production.

CRediT authorship contribution statement

E. Huang-Lin: Writing – original draft, Visualization, Validation, Methodology, Investigation, Formal analysis, Data curation. **S. Cantera:** Writing – review & editing, Validation, Supervision, Project administration, Funding acquisition, Conceptualization. **R. Lebrero:** Writing – review & editing, Validation, Supervision, Project administration, Funding acquisition, Conceptualization.

Declaration of Competing Interest

The authors declare that they have no known competing financial interests or personal relationships that could have appeared to influence the work reported in this paper.

Acknowledgements

This research was funded by the Spanish Ministry of Science and Innovation, Spain (PID2022–139110OA-I00) project CIRCULAR-BIOMED. The financial support from the Department of Education of the Regional Government of Castilla y León and the European Union through FEDER funds (CLU−2025–2–06 and UIC393) are also gratefully acknowledged. The authors also acknowledge the University of Valladolid for the PhD contract of Elisa Huang Lin.

Appendix A. Supporting information

Supplementary data associated with this article can be found in the online version at doi:10.1016/j.jece.2026.122338.

Data availability

Data will be made available on request.

References

[1] D. Etit, S. Meramo, Ó. Ögmundarson, M.K. Jensen, S. Sukumara, Can biotechnology lead the way toward a sustainable pharmaceutical industry? Curr. Opin. Biotechnol. 87 (2024) 103100 https://doi.org/10.1016/j.copbio.2024.103100.
[2] EFPIAThe European Federation of Pharmaceutical Industries and Associations. The pharmaceutical industry in figures Belg. (Eur.)2022, 28.
[3] R.H. Hagenaars, R. Heijungs, A. de Koning, A. Tukker, R. Wang, The greenhouse gas emissions of pharmaceutical consumption and production: an input–output analysis over time and across global supply chains, Lancet Planet. Health 9 (3) (2025) e196–e206, https://doi.org/10.1016/S2542-5196(25)00028-2.
[4] G. Parker, F.A. Miller, Tackling pharmaceutical pollution along the product lifecycle: roles and responsibilities for producers, regulators and prescribers, Pharmacy 12 (6) (2024) 173, https://doi.org/10.3390/pharmacy12060173.
[5] P.-J. Inocencio-García, J.C. Solarte-Toro, C.A. Cardona Alzate, CO2 as raw material for sustainable biorefineries, Waste Biomass-.-. Valoriz. 16 (8) (2025) 3943–3967, https://doi.org/10.1007/s12649-025-03094-6.
[6] R. Konwarh, Embracing sustainable processes in the pharmaceutical industry with green chemistry and engineering, Sustain. Process. Connect (2025), https://doi.org/10.69709/SusProc.2025.133442.
[7] V. Kumar, V. Bansal, A. Madhavan, M. Kumar, R. Sindhu, M.K. Awasthi, P. Binod, S. Saran, Active pharmaceutical ingredient (API) chemicals: a critical review of current biotechnological approaches, Bioengineered 13 (2) (2022) 4309–4327, https://doi.org/10.1080/21655979.2022.2031412.
[8] D. Lips, Fuelling the future of sustainable sugar fermentation across generations, Eng. Biol. 6 (1) (2022) 3–16, https://doi.org/10.1049/enb2.12017.
[9] E. Orsi, P.I. Nikel, L.K. Nielsen, S. Donati, Synergistic investigation of natural and synthetic C1-trophic microorganisms to foster a circular carbon economy, Nat. Commun. 14 (1) (2023) 6673, https://doi.org/10.1038/s41467-023-42166-w.
[10] R. Takors, M. Kopf, J. Mampel, W. Bluemke, B. Blombach, B. Eikmanns, F. R. Bengelsdorf, D. Weuster-Botz, P. Dürre, Using gas mixtures of CO, CO $_2$ and H $_2$ as microbial substrates: the do's and don'ts of successful technology transfer from laboratory to production scale, Microb. Biotechnol. 11 (4) (2018) 606–625, https://doi.org/10.1111/1751-7915.13270.
[11] S. Stegman, C. Melkonian, D. Tamarit, E. Huang-Lin, R. Lebrero, S. Cantera, Prospective bioconversion of CO2 and CO into fine chemicals via halophilic purple phototrophic bacteria, Rev. Environ. Sci. Bio/Technol. 24 (1) (2025) 29–41, https://doi.org/10.1007/s11157-025-09722-w.
[12] C. Zhang, Q. Fei, R. Fu, M. Lackner, Y.J. Zhou, T. Tan, Economic and sustainable revolution to facilitate one-carbon biomanufacturing, Nat. Commun. 16 (1) (2025) 4896, https://doi.org/10.1038/s41467-025-60247-w.
[13] G. Gong, B. Wu, L. Liu, J. Li, Q. Zhu, M. He, G. Hu, Valorization of waste streams and C1 gases for sustainable food nutrients and value-added compounds production: Acetate as a promising intermediate, Sci. Total Environ. 893 (2023) 164795, https://doi.org/10.1016/j.scitotenv.2023.164795.
[14] Y. Wu, Y. Yuan, C. Xia, T.A. Alahmadi, S.A. Alharbi, M. Sekar, A. Pugazhendhi, Production of waste tyre pyrolysis oil as the replacement for fossil fuel for diesel engines with constant hydrogen injection via air intake manifold, Fuel 355 (2024) 129458, https://doi.org/10.1016/j.fuel.2023.129458.
[15] N. Ahmad, F. Ahmad, I. Khan, A.D. Khan, Studies on the Oxidative Removal of Sodium Thiosulfate from Aqueous Solution, Arab. J. Sci. Eng. 40 (2) (2015) 289–293, https://doi.org/10.1007/s13369-014-1473-0.
[16] B.E. Valdez-Guzmán, J.B. Velázquez-Fernández, L.A. Arellano-García, Bioprocessing of reduced sulfur compounds enhanced by treated wastewater with an alkaliphilic sulfur-oxidizing microbial consortium, Bioremediation J. (2024) 1–15, https://doi.org/10.1080/10889868.2024.2407240.
[17] B. Peng, H. Peng, R.E. Speight, Recycling CO2 into bioingredients: towards synthetic photo/litho-mixotrophy, Trends Biotechnol. (2025), https://doi.org/10.1016/j.tibtech.2025.10.013.
[18] W. Park, S. Cha, J.-S. Hahn, Advancements in Biological Conversion of C1 Feedstocks: Sustainable Bioproduction and Environmental Solutions, ACS Synth. Biol. 13 (12) (2024) 3788–3798, https://doi.org/10.1021/acssynbio.4c00519.
[19] E. Huang-Lin, R. Lebrero, S. Cantera, Continuous valorization of carbon dioxide into the fine chemical ectoine by *Hydrogenovibrio marinus*: a new strategy for pharmaceutical production, Environ. Sci. & Technol. (2025), https://doi.org/10.1021/acs.est.4c12259.
[20] Y. Feng, M. Qiu, L. Shao, Y. Jiang, W. Zhang, W. Jiang, F. Xin, M. Jiang, Strategies for the biological production of ectoine by using different chassis strains, Biotechnol. Adv. 70 (2024) 108306, https://doi.org/10.1016/j.biotechadv.2023.108306.
[21] P. Kadam, M. Khisti, V. Ravishankar, V. Barvkar, D. Dhotre, A. Sharma, Y. Shouche, S. Zinjarde, Recent advances in production and applications of ectoine, a

compatible solute of industrial relevance, Bioresour. Technol. 393 (2024) 130016, https://doi.org/10.1016/j.biortech.2023.130016.
[22] M. Shaikhpour, Anticancer and Apoptotic Effects of Ectoine and Hydroxyectoine on Non-Small Cell Lung Cancer cells: An in-vitro Investigation, Multidiscip. Cancer Investig. 03 (2) (2019) 14–19, https://doi.org/10.30699/acadpub.mci.3.2.14.
[23] P. Ruiz-Ruiz, P. Mohedano-Caballero, J. de Vrieze, Ectoine production through a marine methanotroph-microalgae culture allows complete biogas valorization, J. Environ. Manag. 375 (2025) 124223, https://doi.org/10.1016/j.jenvman.2025.124223.
[24] Z. Lei, X. Chen, L. Yuan, J. Wu, J. Yao, Metabolic Control for High-Efficiency Ectoine Synthesis in Engineered *Escherichia coli*, ACS Synth. Biol. 14 (8) (2025) 3177–3185, https://doi.org/10.1021/acssynbio.5c00330.
[25] E. Huang-Lin, D. Tamarit, R. Lebrero, S. Cantera, Guyparkeria halophila: Novel cell platform for the efficient valorization of carbon dioxide and thiosulfate into ectoine, Bioresour. Technol. 408 (2024) 131152, https://doi.org/10.1016/j.biortech.2024.131152.
[26] S. Cantera, F. di Benedetto, B.F. Tumulero, D.Z. Sousa, Microbial conversion of carbon dioxide and hydrogen into the fine chemicals hydroxyectoine and ectoine, Bioresour. Technol. 374 (2023) 128753, https://doi.org/10.1016/j.biortech.2023.128753.
[27] J.L. Houghton, D.I. Foustoukos, T.M. Flynn, C. Vetriani, A.S. Bradley, D.A. Fike, Thiosulfate oxidation by *Thiomicrospira thermophila*: metabolic flexibility in response to ambient geochemistry, Environ. Microbiol. 18 (9) (2016) 3057–3072, https://doi.org/10.1111/1462-2920.13232.
[28] R. Baird, L. Bridgewater. Standard Methods for the Examination of Water and Wastewater, (23rd ed.)., American Public Health Association, 2017.
[29] T. Magoč, S.L. Salzberg, FLASH: fast length adjustment of short reads to improve genome assemblies, Bioinformatics 27 (21) (2011) 2957–2963, https://doi.org/10.1093/bioinformatics/btr507.
[30] N.A. Bokulich, S. Subramanian, J.J. Faith, D. Gevers, J.I. Gordon, R. Knight, D. A. Mills, J.G. Caporaso, Quality-filtering vastly improves diversity estimates from Illumina amplicon sequencing, Nat. Methods 10 (1) (2013) 57–59, https://doi.org/10.1038/nmeth.2276.
[31] R.C. Edgar, B.J. Haas, J.C. Clemente, C. Quince, R. Knight, UCHIME improves sensitivity and speed of chimera detection, Bioinformatics 27 (16) (2011) 2194–2200, https://doi.org/10.1093/bioinformatics/btr381.
[32] H. Wickham, ggplot2, Springer, New York, 2009, https://doi.org/10.1007/978-0-387-98141-3.
[33] M. Liu, H. Liu, M. Shi, M. Jiang, L. Li, Y. Zheng, Microbial production of ectoine and hydroxyectoine as high-value chemicals, Microb. Cell Factor. 20 (1) (2021) 76, https://doi.org/10.1186/s12934-021-01567-6.
[34] M.C.Y. Lau Vetter, B. Huang, L. Fenske, J. Blom, Metabolism of the Genus Guyparkeria Revealed by Pangenome Analysis, Microorganisms 10 (4) (2022) 724, https://doi.org/10.3390/microorganisms10040724.
[35] S. Ruan, Y. Jiang, A. Wang, X. Zhang, Y. Lin, S. Liang, Carbon sequestration pathways in microorganisms: Advances, strategies, and applications, Eng. Microbiol. 5 (2) (2025) 100196, https://doi.org/10.1016/j.engmic.2025.100196.
[36] T.N.-D. Cao, S.W. Snyder, Y.-I. Lin, Y.J. Lin, S. Negi, S.-Y. Pan, Unraveling the potential of electrochemical pH-swing processes for carbon dioxide capture and utilization, Ind. Eng. Chem. Res. 62 (49) (2023) 20979–20995, https://doi.org/10.1021/acs.iecr.3c02183.
[37] R. Boden, Reclassification of Halothiobacillus hydrothermalis and Halothiobacillus halophilus to Guyparkeria gen. nov. in the Thioalkalibacteraceae fam. nov., with emended descriptions of the genus Halothiobacillus and family Halothiobacillaceae, Int. J. Syst. Evolut. Microbiol. 67 (10) (2017) 3919–3928, https://doi.org/10.1099/ijsem.0.002222.
[38] F. Orhan, A. Akıncıoğlu, E. Ceyran, Ectoine production from a novel bacterial strain and high-purity purification with a cost-effective and single-step method, J. Biotechnol. 388 (2024) 24–34, https://doi.org/10.1016/j.jbiotec.2024.04.003.
[39] R. Ye, Q. Jin, B. Bohannan, J.K. Keller, S.A. McAllister, S.D. Bridgham, pH controls over anaerobic carbon mineralization, the efficiency of methane production, and methanogenic pathways in peatlands across an ombrotrophic–minerotrophic gradient, Soil Biol. Biochem. 54 (2012) 36–47, https://doi.org/10.1016/j.soilbio.2012.05.015.
[40] M. Silver, O. Dinardo, Factors affecting oxidation of thiosalts by thiobacilli, Appl. Environ. Microbiol. 41 (6) (1981) 1301–1309, https://doi.org/10.1128/aem.41.6.1301-1309.1981.
[41] D.M. Arias, E. Uggetti, M.J. García-Galán, J. García, Nutrients and biomass dynamics in photo-sequencing batch reactors treating wastewater with high nutrients loadings, Ecol. Eng. 119 (2018) 35–44, https://doi.org/10.1016/j.ecoleng.2018.05.016.
[42] C. Zhan, T. Liu, Y. Chen, Y. Zhu, X. Li, J. Liu, Q. Zhao, X. Chen, A. Zeng, Advancing synthetic biology for sustainable one-carbon biomanufacturing, Green. Carbon (2025), https://doi.org/10.1016/j.greenca.2025.08.003.
[43] S. Cantera, V. Phandanouvong-Lozano, C. Pascual, P.A. García-Encina, R. Lebrero, A. Hay, R. Muñoz, A systematic comparison of ectoine production from upgraded biogas using Methylomicrobium alcaliphilum and a mixed haloalkaliphilic consortium, Waste Manag. 102 (2020) 773–781, https://doi.org/10.1016/j.wasman.2019.11.043.
[44] Q. Zhao, S. Li, P. Lv, S. Sun, C. Ma, P. Xu, H. Su, C. Yang, High ectoine production by an engineered Halomonas hydrothermalis Y2 in a reduced salinity medium, Microb. Cell Factor. 18 (1) (2019) 184, https://doi.org/10.1186/s12934-019-1230-x.
[45] A.E. Onraedt, B.A. Walcarius, W.K. Soetaert, E.J. Vandamme, Optimization of Ectoine Synthesis through Fed-Batch Fermentation of Brevibacterium epidermis, Biotechnol. Prog. 21 (4) (2008) 1206–1212, https://doi.org/10.1021/bp0500967.
[46] I. Putu Parwata, D. Wahyuningrum, S. Suhandono, R. Hertadi, Production of ectoine by *Halomonas elongata* BK-AG25 using osmotic shock technique, IOP Conference Series Earth Environmental Science 209 (2018) 012017, https://doi.org/10.1088/1755-1315/209/1/012017.
[47] Q. Hu, S. Sun, Z. Zhang, W. Liu, X. Yi, H. He, N.S. Scrutton, G.-Q. Chen, Ectoine hyperproduction by engineered Halomonas bluephagenesis, Metab. Eng. 82 (2024) 238–249, https://doi.org/10.1016/j.ymben.2024.02.010.
[48] P. Fatollahi, M. Ghasemi, F. Yazdian, A. Sadeghi, Ectoine production in bioreactor by Halomonas elongata DSM2581: Using MWCNT and Fe-nanoparticle, Biotechnol. Prog. 37 (1) (2021), https://doi.org/10.1002/btpr.3073.
[49] A. Radha, I.N. Najar, N. Nekkala, S. Sharma, V. Sharma, R. Bhanwaria, V. Kumar, Efficient production of ectoine using isolated *Halomonas smyrnensis* IIIM VA-6 at the reduced salinity approach, FEMS Microbiol. Lett. 373 (2026), https://doi.org/10.1093/femsle/fnag001.
[50] M. Liu, H. Liu, M. Shi, M. Jiang, L. Li, Y. Zheng, Microbial production of ectoine and hydroxyectoine as high-value chemicals, Microb. Cell Factor. 20 (1) (2021) 76, https://doi.org/10.1186/s12934-021-01567-6.
[51] W. van Hecke, R. Bockrath, H. de Wever, Effects of moderately elevated pressure on gas fermentation processes, Bioresour. Technol. 293 (2019) 122129, https://doi.org/10.1016/j.biortech.2019.122129.
[52] K. Ying, M.K.H. Al-Mashhadani, J.O. Hanotu, D.J. Gilmour, W.B. Zimmerman, Enhanced Mass Transfer in Microbubble Driven Airlift Bioreactor for Microalgal Culture, Engineering 05 (09) (2013) 735–743, https://doi.org/10.4236/eng.2013.59088.
[53] Y. Wu, Z. Zeng, R. Teng, J. Yu, G. Guo, P. Huang, Z. Huang, S. Deng, pH-dependent overestimation of heavy metals mobility risk in soils: Implications for soil quality assessment, J. Hazard. Mater. 501 (2026) 140792, https://doi.org/10.1016/j.jhazmat.2025.140792.
[54] R. Ahmed, The Role of cGMP in the manufacturing unit of a pharmaceutical industry, Radinka J. Health Sci. 2 (2) (2024) 242–253, https://doi.org/10.56778/rjhs.v2i2.361.
[55] K. Pilaniya, H. Chandrawanshi, U. Pilaniya, P. Manchandani, P. Jain, N. Singh, Recent trends in the impurity profile of pharmaceuticals, J. Adv. Pharm. Technol. & Res. 1 (3) (2010) 302, https://doi.org/10.4103/0110-5558.72422.
[56] D. Xie, Continuous biomanufacturing with microbes — upstream progresses and challenges, Curr. Opin. Biotechnol. 78 (2022) 102793, https://doi.org/10.1016/j.copbio.2022.102793.
[57] M. Parroquin-Gonzalez, J. Winterburn, Continuous bioreactor production of polyhydroxyalkanoates in Haloferax mediterranei, Front. Bioeng. Biotechnol. 11 (2023), https://doi.org/10.3389/fbioe.2023.1220271.
[58] H.S. Ng, P.-K. Wan, A. Kondo, J.-S. Chang, J.C.-W. Lan, Production and Recovery of Ectoine: A Review of Current State and Future Prospects, Processes 11 (2) (2023) 339, https://doi.org/10.3390/pr11020339.
[59] V. Pérez, J.L. Moltó, R. Lebrero, R. Muñoz, Ectoine production from biogas: a sensitivity analysis. Effect of local commodity prices, economy of scale, market trends and biotechnological limitations, J. Clean. Prod. 369 (2022) 133440, https://doi.org/10.1016/j.jclepro.2022.133440.